 CMC, vol.7, no.2, pp.59-79, 2008

Cracking and Creep Role in Displacements at Constant Load: Concrete Solids in Compression

E. Ferretti[1] **and A. Di Leo**[1]

Abstract: The main assumption on the basis of the identifying model of the effective law, developed by the Author, is the impossibility of considering the specimen as a continuum, when an identifying procedure from load-displacement to stress-strain in uniaxial compression is attempted. Actually, a failure mechanism with propagation of a macro-crack was found to activate from the very beginning of the uniaxial compression test forth. This leads to considering the acquired displacements as composed by two quotes: one constitutive, due to the material strain, and one of crack opening. Since the ratio between these two quotes is not constant during the compression test, the properties of the displacement field (which attains to structural properties) cannot be transposed to the strain field (which attains to material properties) through a mere scale factor. In this context, also creep takes on a different meaning, in the sense that time-dependence is an effect observed in the displacement field that does not necessarily correspond to a property of the strain field, i.e., the creep. In other words, it is not possible to exclude a-priori that the time-dependence of displacements is induced by crack propagation alone. A time-dependent motion of crack opening could activate and affect the displacements acquisition. The aim of the present work is to investigate the role played in displacement time-dependence both by creep and crack propagation. Results of an experimental program are presented here, stating the strict relationship existing between the increasing of displacement and the propagation of cracks at constant load.

Keyword: Damage, Creep, Constitutive parameters, Identification, Microseismic analysis.

[1] DISTART, Scienza delle Costruzioni, Facoltà di Ingegneria, Alma Mater Studiorum, Università degli Studi di Bologna, Viale Risorgimento 2, 40136, Bologna, ITALY.

1 Introduction

The present study is part of a research on the identification of the constitutive parameters of concrete. As it is well known, the stress–strain relationship of concrete in uniaxial compression is traditionally derived from the experimental load–displacement relationship, N–u, of concrete specimens in uniaxial compression, where u is the relative displacement between the platens of the testing machine, through a scale factor (Figure 1). Actually, it is a common practice to define the stress and strain at a point as the average stress $\overline{\sigma}$ on the nominal area of the specimen, A_n, and the average strain $\overline{\varepsilon}$ on the specimen height, L, respectively:

$$\sigma = \overline{\sigma} = \frac{N}{A_n}; \tag{1}$$

$$\varepsilon = \overline{\varepsilon} = \frac{\Delta L}{L} = \frac{u}{L}. \tag{2}$$

Consequently, the specimen is considered as uniformly stressed and strained. Nevertheless, large reductions of the effective cross-sectional area occur in a concrete specimen in uniaxial compression, due to the propagation of macro-cracks through the specimen from the very beginning of the test [Ferretti (2001; 2004a)]. In cylindrical specimens, these cracks isolate an inner core of bi-conic shape (Figure 3).

The outer part of the specimen, the one located around the inner core, is expelled along the radial direction (scheme on the middle cross-section in Figure 2). This results in splitting of the outer part into several portions, with propagation of sub-vertical macro-cracks on the external surface of the specimen (Figure 2).

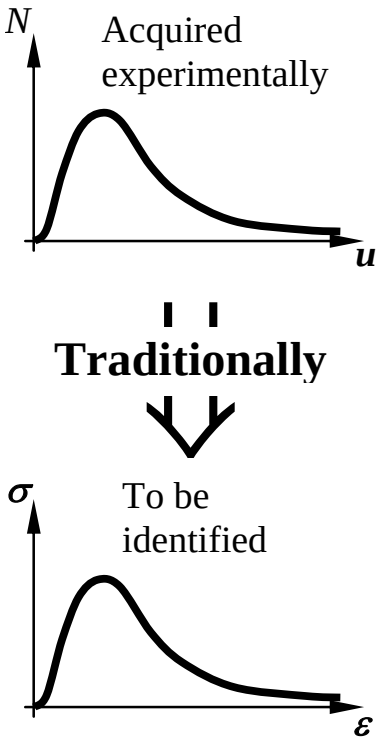

Figure 1: Traditional identification of the $\sigma - \varepsilon$ relationship in uniaxial compression

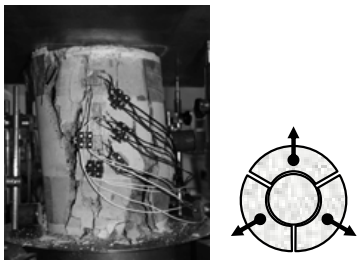

Figure 2: Concrete specimen at the end of the test, and splitting-scheme on the middle cross-section

Figure 3: Concrete specimen at the end of the test, after removal of the outer part

Due to the cylindrical geometry, each longitudinal section of the specimen shown in Figure 2 is subjected to plane strain and deforms as a compressed plate. In Nemat-Nasser and Horii (1982), it was suggested that axial splitting in uniaxially compressed plates of brittle materials stems from the formation of tension cracks developed at the tips of pre-existing cracks, because of the relative sliding of their faces. We can thus expect that the bi-conic macro-cracks are tension cracks, which grow as the compression load increases.

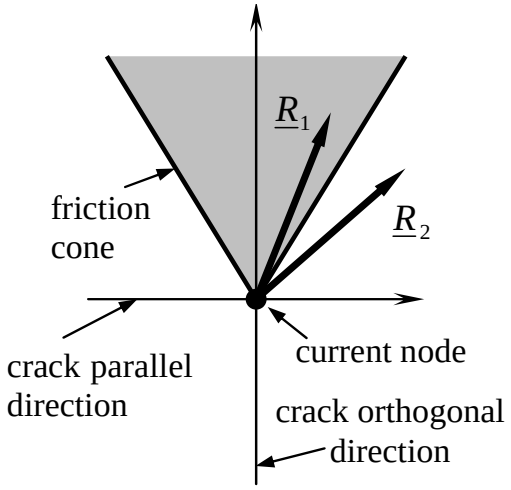

Figure 4: Example of the validity ($\underline{R}_1$) and of non-validity ($\underline{R}_2$) of the no relative slip assumption

In Ferretti (2003), the propagation of the bi-conic macro-cracks has been modeled as a Mixed-Mode crack propagation problem, with Mode I of crack opening prevailing near the platens of the testing machine and Mode II of crack sliding prevailing near the crack tip. A friction model analogous to that employed in Nemat-Nasser and Horii (1982) is used to asses the forces acting across the crack faces in Mode II loading. Relative slip can only take place if the constraining reaction forces for nodes in Mode II loading lie on the surface of the friction cone (Figure 4). As can be seen in Figure 5b, a tensile state of stress originates in front of the crack tip, supporting the idea that the splitting process is more likely the product of a tensile than of a shear process [Hallbauer Wagner and Cook (1973); Nemat-Nasser and Horii (1982)]. Due to splitting, the outer part of the specimen looses its load-carrying capability, while the inner core continues to carry load as the bi-conic cracks propagate. The final shape of the inner core, resulting from removal of the non-collaborating material, is shown in Figure 3. No evident crack propagation seems to afflict this core. Thus, it represents the resistant structure at the end of the compres-

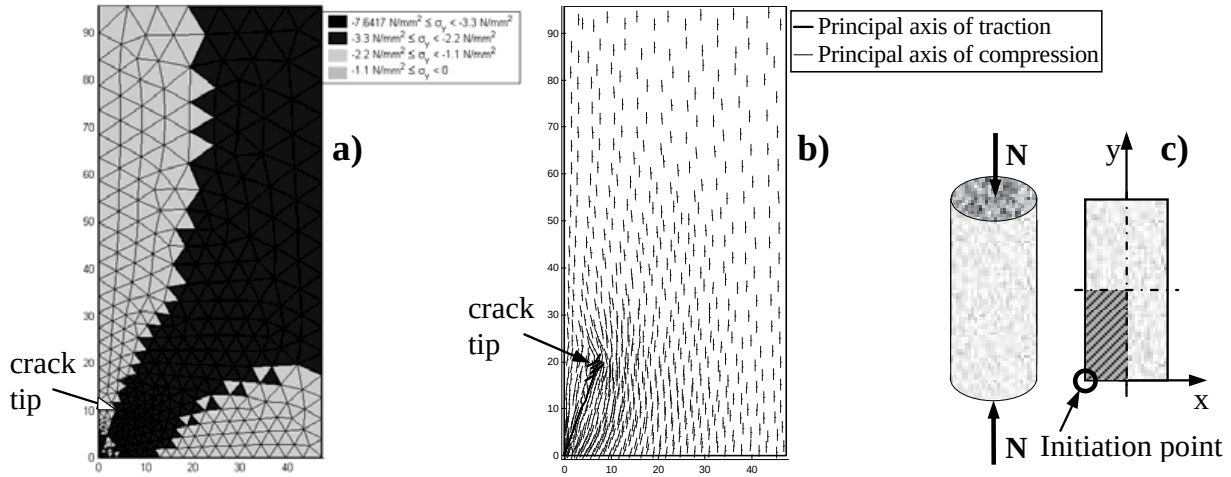

Figure 5: a) Stress field after short cracking; b) Stress axes; c) Loading scheme and modeled domain

sion test. Since the propagation of bi-cone shaped crack does not characterize the final stage only, but progresses with load from the very beginning of the test [Soga Mizutani Spetzler and Martin (1978)], the resistant structure gradually evolves from the one coinciding with the specimen and the one in Figure 3. A qualitative representation of the resistant structure at an intermediate step of loading is given by the darker part of the longitudinal section in Figure 5a.

We may assume that, after each crack propagation, the material properties do not vary, while the structural response can vary drastically, since a lower amount of material collaborates to carry the applied load. Actually, the modification of resistant structure involves a decrease of the resistant area, A_{res}, such as happens with steel tensioned until softening [Candra Wright and Albrecht (2002)], which largely influences the structural behavior of the specimen. An identifying model, and not a scale factor, is thus needed in order to derive the $\sigma - \varepsilon$ law, which attains to the material, from the experimental $N - u$ law, which attains to the structure.

The main consequence of assuming that the $\sigma - \varepsilon$ and the $N - u$ laws are not related by a scale factor is that these two curves may not be identical in shape (Figure 6). In particular, the $\sigma - \varepsilon$ curve of displacement-controlled compression tests on standard cylindrical specimens of concrete-like materials ($D = 15$ cm; $L = 30$ cm) may not have the softening behavior of the experimental $N - u$ curve, that is, the decline of load at increasing displacement, after the maximum load is reached, may not involve a decline of stress at increasing strain. The actual shape of the $\sigma - \varepsilon$ law in uniaxial compression can only be known if the law according to which the resistant area decreases is known.

The need of evaluating a load-carrying reduced area in concrete-like materials was pointed out also in Bergan (1983), Hegemier and Read (1983), Sandler and Wright (1983), Wu and Freud (1983), Dresher and Vardoulakis (1982), Hudson Brown and Fairhurst (1971). All these studies share the common idea of the non constitutive nature of strain-softening, that is, the decline of stress at increasing strain. In particular, Hudson Brown and Fairhurst (1971) explained the softening $N - u$ ($\overline{\sigma} - \overline{\varepsilon}$) curves, observed for large L/D ratios, on the basis of the slabbing and shear failure, leading to large reductions in the effective cross-sectional area. In their opinion, strain-softening is an apparent affect, due to scaling the applied force by the original cross-sectional (Eq. (1)) rather than the actual cross-sectional area (Figure 7).

The monotonic non-decreasing behavior of the $N - u$ ($\overline{\sigma} - \overline{\varepsilon}$) curves of concrete-like solids with small L/D ratios is in well agreement with the assumptions of Hudson Brown and Fairhurst (1971). Actually, for small L/D ratios the re-

duction in cross-sectional area is very small and the $\overline{\sigma}-\overline{\varepsilon}$ curves are close to the true stress-strain curves, that is, they are still monotonic non-decreasing (Figure 7). Nevertheless, none of the studies of the '70s and '80s mentioned above related the problem of the existence of strain-softening in concrete to experimental procedures. They treated the problem from physical and mathematical points of view only, since it was estimated [Hegemier and Read (1983)] to be extremely difficult, if not impossible, to track the effective cross-sectional area experimentally at each stage of the failure process.

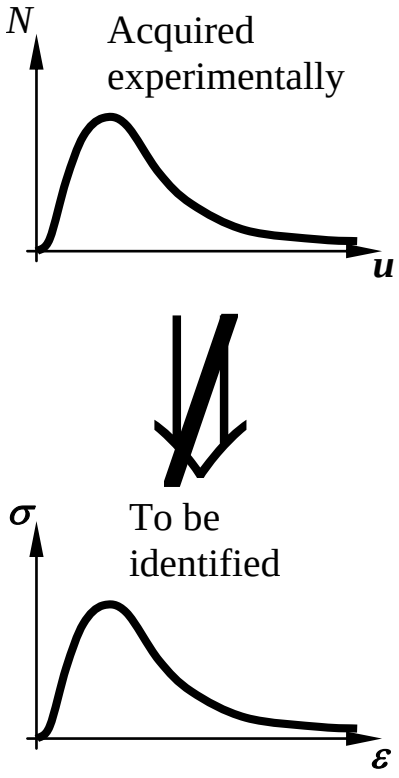

Figure 6: Scheme of the relationship between load-displacement and stress-strain relationships

The impossibility of achieving a new constitutive proposal was actually the main reason for which this field of research rapidly fell out of favor. On the contrary, in Ferretti (2001), the idea of the non constitutive nature of strain-softening is supported by a new identification proposal for constitutive properties, the identifying model of the effective law. A discussion on how the existence and mathematical well-posedness of strain-softening is still an open question is provided in Ferretti (2005).

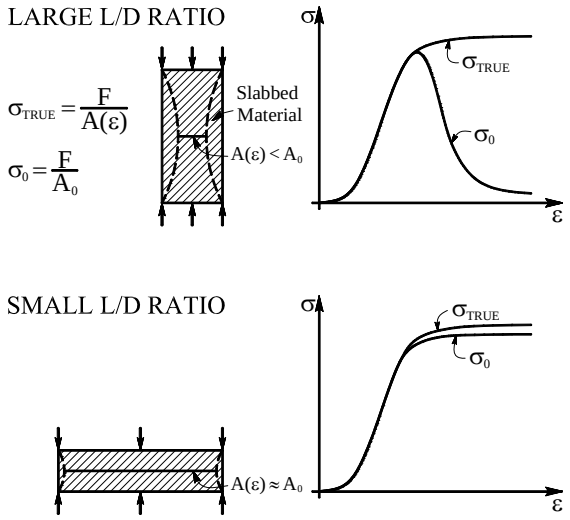

Figure 7: Effect of stress definition on the shape of the stress-strain curve, with $A_0 = A_n$ and $\sigma_0 = \overline{\sigma}$ [Hudson Brown and Fairhurst (1971)]

2 The identifying model of the effective law

2.1 Evaluation of effective stress and effective strain

The aim of the identifying model of the effective law is the evaluation of the load-carrying reduced area, A_{res}, in order to identify the average stress and strain acting on A_{res}. In accordance with the experimental evidence (Section 1, Figure 3), the model assumes that concrete cylinders in uniaxial compression fail with propagation of the macro-crack shown in Figure 8, isolating an inner core of intact material [Ferretti (2001)].

As previously stated, it is extremely difficult to track A_{res} experimentally at each stage of the failure process. More simple is to estimate the percentage decrease of A_{res}, d:

$$d = \frac{A_n - A_{res}}{A_n}. \tag{3}$$

In Eq. (3), d is a scalar, continuously varying from 0 (virgin state) to 1 (failure). By means of Eq. (3), the resistant area can be expressed as follows:

$$A_{res} = A_n\,(1-d)\,. \tag{4}$$

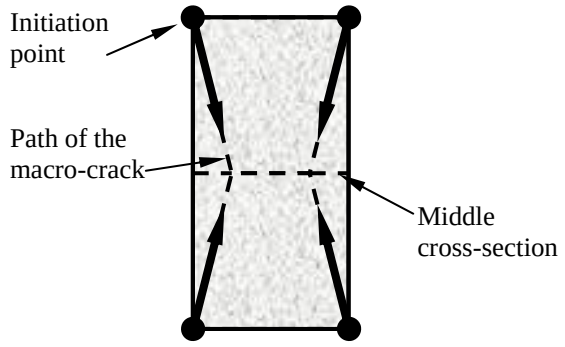

Figure 8: Failure model in concrete cylindrical specimens

Eq. (4) is the same as the one proposed in the scalar formulation of Continuum Mechanics with damage. Nevertheless, the point of view has changed. In Continuum Mechanics with scalar damage, d is a damage and is a material property. Here, d is a measure of how much crack propagation affects the resistant area and is a structural property. Moreover, d is not estimated by means of analytical formulations, but is evaluated on the basis of two experimental laws. The first law, d_1 [Ferretti (2001)], relates d to the dissipated energy at the current point, W_d, and the total dissipated energy, $W_{d,t}$ (Figure 9):

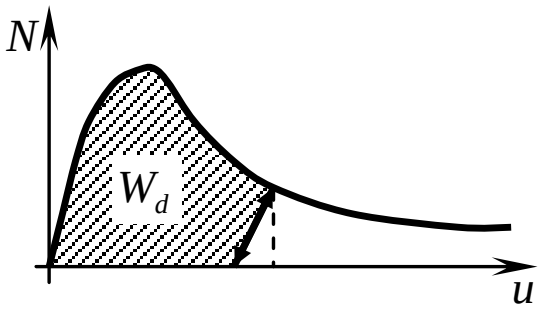

Figure 9: Evaluation of W_d at the general load-step

$$d_1 = \frac{W_d}{W_{d,t}}. \tag{5}$$

where $W_{d,t}$ is the value of W_d at the final stage. This quantity is used in Eq. (5) as reference value

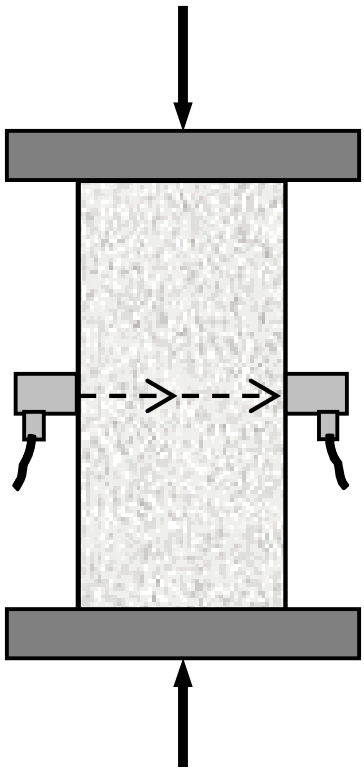

Figure 10: Test set-up for the acquisition of d_2

for defining d. Thus, $W_{d,t}$ must be a known value, while it is difficult to acquire experimentally. Consequently, a second law with a known reference value is needed. The second law we used is the microseismic law of Daponte and Olivito (1989):

$$d_2 = 1 - \frac{V}{V_0}, \tag{6}$$

where V is the compressional wave velocity at the current point and V_0 is the initial velocity of the compressional waves, in a microseismic analysis performed during loading. The reference value is V_0, easily acquirable before the compression test begins. In order to acquire d_2 in continuum, two probes for microseismic analysis have been glued at the ends of a diameter of the middle cross-section (Figure 10).

By comparison between the values of A_{res} evaluated by means of the energetic and microseismic laws (Figure 11), it is possible to calibrate $W_{d,t}$. The d_1, d_2 versus the average strain curves

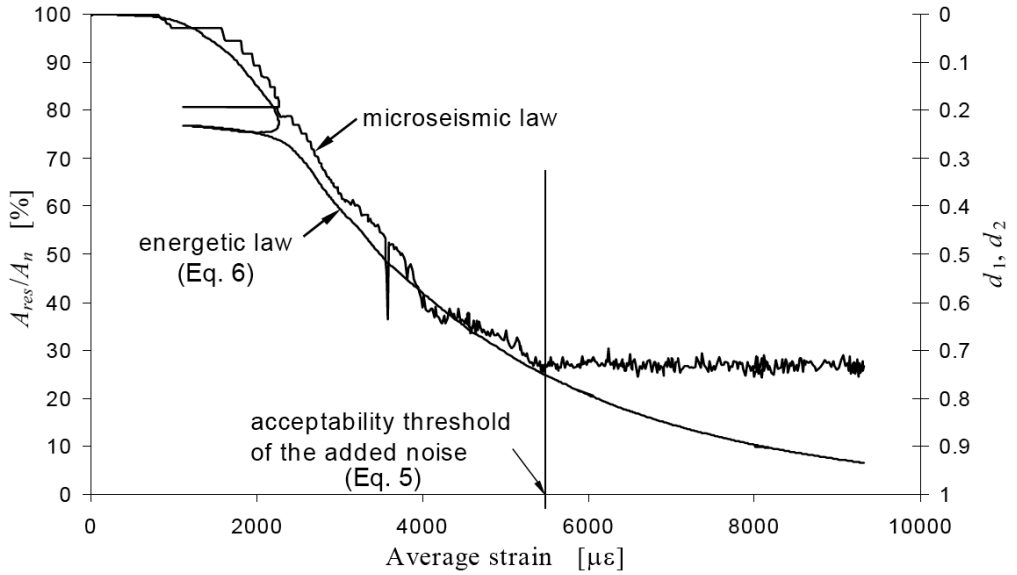

Figure 11: Comparison between the energetic (Eq. (5)) and microseismic (Eq. (6)) laws [Ferretti (2004a)]

are plotted in Figure 11. It can be appreciated how a value of strain exists, beyond which the noise due to crack propagation disturbs the microseismic survey so much that the variations of the microseismic signal cannot be appreciated any longer (Figure 11). This value of strain has been termed the acceptability threshold of the added noise. Due to the existence of an acceptability threshold, the survey field of d_2 is limited. On the contrary, the survey field of d_1 is not affected by any limitation. Thus, only d_1 is useful for identifying the effective properties, while d_2 is used for calibration. The law of the effective properties that follows from the calibration is highly reproducible for each specimen geometry [Ferretti (2001; 2004a)], with a low data dispersion.

The slope of the curves in Figure 11 gives the rate of cracking with the average strain. The flex points in Figure 11 correspond to the peak axial load [Ferretti (2004a)]. This means that, according to the results given by optical microscopy, acoustic emission, scanning electron microscopy, and other methods (see Horii and Nemat-Nasser (1985) for discussions and references), the identifying model of the effective law shows that, as the load is increased up to the peak axial load, the rate of cracking accelerates. The maximum rate of cracking is reached just at the peak axial load. The subsequent decreasing of cracking rate is due to the specimen unloading.

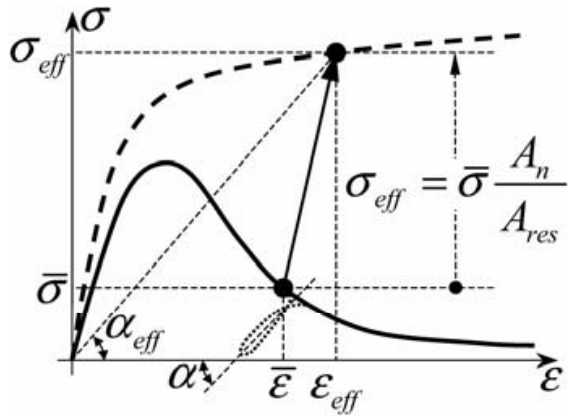

Figure 12: Identification of the effective quantities starting from the average quantities [Ferretti (2004a)]

The average stress acting on A_{res}, the effective stress σ_{eff}, results from the ratio between the applied load, N, and A_{res} (Figure 12):

$$\sigma_{eff} = \frac{N}{A_{res}} = \frac{N}{A_n}\frac{A_n}{A_{res}} = \overline{\sigma}\frac{A_n}{A_{res}}. \tag{7}$$

σ_{eff} represents the actual stress at a point of the material.

The effective strain at a point of the material, ε_{eff},

is defined as:

$$\varepsilon_{eff} = \sigma_{eff}/E_s, \tag{8}$$

where $E_s = E_s(\overline{\varepsilon}) = \tan\alpha_{eff} = A_n/A_{res}\tan\alpha$ is the average slope of the unloading-reloading cycle at the current point, in the $\sigma_{eff} - \varepsilon_{eff}$ curve (Figure 12). E_s characterizes the effective instantaneous stiffness of the material, since it can be experimentally appreciated that no evolution of the failure pattern occurs during unloading-reloading [Ferretti (2004a)].

2.2 Main findings

The complete identification procedure for concrete and an experimental program on cylindrical specimens of radius R and diameter D, for a L/D ratio varying from 1.5 to 4 (Figure 13), have been described in Ferretti (2001; 2004a). Here, we only need to recall that:

- A_{res} starts to decrease as soon as the average strain becomes different from zero (Figure 11 and Figure 13). This confirms that the macro-crack initiates at the very beginning of the test [Soga Mizutani Spetzler and Martin (1978)].

- d_1 is size-effect sensitive since, the highest is the L/D ratio, the highest is d_1 for each load-step (Figure 13).

- The identified effective law, $\sigma_{eff} - \varepsilon_{eff}$, is monotonic non-decreasing (Figure 15), in spite of the softening behavior of the $\overline{\sigma} - \overline{\varepsilon}$ curves (Figure 14).

- The curves of the effective properties are size-effect insensitive (Figure 15), while not the curves of the average properties (Figure 14), as it is well known.

- The ratio $-\varepsilon_r/\varepsilon_l$, with ε_r the radial strain acquired into the inner core by means of fiber optic sensors (FOSs; Figure 16) and $\varepsilon_l = \Delta L/L$ the longitudinal strain, is constantly close to the static Poisson's ratio ($\nu = -\varepsilon_r/\varepsilon_l$; Figure 17). On the contrary, the traditional procedure for the identification of ν, with ε_r acquired as the average circumferential strain, ε_c, on the middle cross-section (Figure 16),

  $$\varepsilon_r = \Delta R/R = 2\pi\Delta R/2\pi R = \varepsilon_c \tag{9}$$

  gives an increasing ν, which comes out of the validity range ($0 < \nu < 0.5$).

- The volumetric curve $N - \varepsilon_\vartheta$ with the volumetric strain

  $$\begin{aligned}\varepsilon_\vartheta = I_{1\varepsilon} &= \varepsilon_1 + \varepsilon_2 + \varepsilon_3 \\ &= \varepsilon_l + \varepsilon_r + \varepsilon_c = \varepsilon_l + 2\varepsilon_r\end{aligned} \tag{10}$$

  obtained on the basis of the FOS-acquired radial strain, is in the negative field (Figure 18). On the contrary, if ε_r is acquired as the average ε_c, the curve $N - \varepsilon_\vartheta$ is, mostly, in the positive field [Brace Paulding and Scholz (1966); Di Leo Di Tommaso and Merlari (1979); Figure 18), involving volume increase (dilatancy).

The size-effect insensitivity of the effective law gives a strong validation to the identifying model of the effective law.

As far as the findings on ν and ε_ϑ are concerned, they can be explained on the basis of the deformed configuration shown in Figure 16, in the sense that the term $2\pi\Delta R$ in Eq. (9) is composed by two quotes: displacements due to the material strain and rigid displacements due to crack openings. Thus, the circumferential strain gauge does not indeed provide a strain acquisition and the first and third equalities in Eq. (9) are no longer valid from the moment in which the macro-crack starts to propagate forth. Since the macro-crack starts to propagate soon after the test begins, Eq. (9) ceases to be valid from the very beginning of the compression test. Therefore, the variation of circumference length cannot be employed for deriving the relationship between radial strain and applied load. On the contrary, the acquisitions into the inner core are quite representative of ε_r, since they are not affected by crack openings. It may be concluded that the Poisson's ratio of concrete does not change during loading.

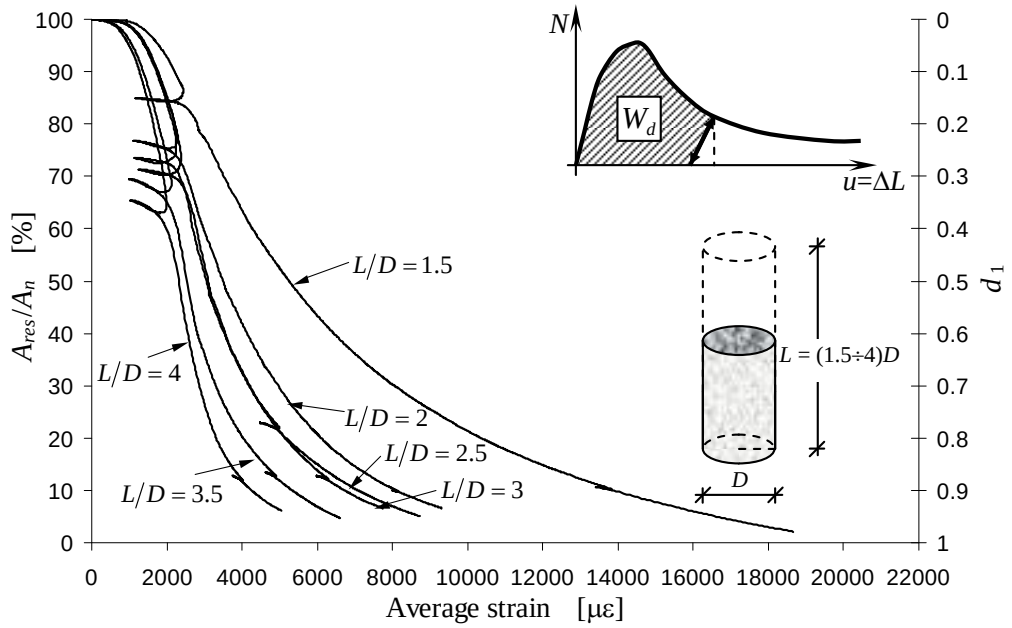

Figure 13: Percentage resistant area and d_1 versus average strain, for variable L/D ratio [Ferretti (2004a)]

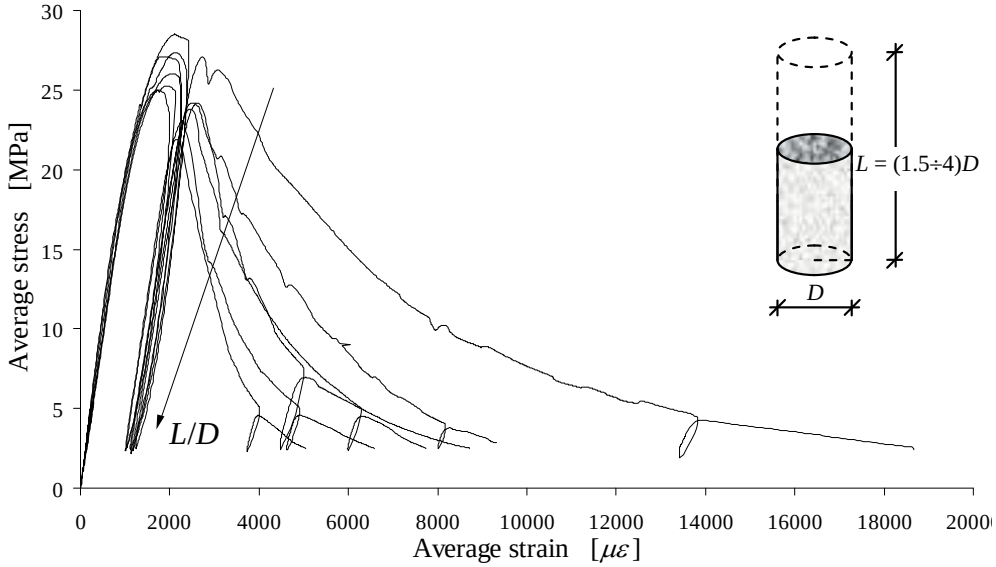

Figure 14: Softening behavior and size-effect for the $\overline{\sigma} - \overline{\varepsilon}$ diagrams [Ferretti (2004a)]

Since the radial strain derived as the average ε_c is affected by crack openings, while not the one acquired into the inner core, even for the relationship $N - \varepsilon_\vartheta$ the curve following from FOS acquisitions is more representative of the actual concrete behavior than the traditional curve is. In this case, one can assert that concrete never exhibits dilatancy. In accordance with the findings of Brace Paulding and Scholz (1966), concrete dilatancy is only an apparent effect, due to an experimental technique, which inadequately evaluates the influence on acquired data of a failure mechanism with crack openings. That is, concrete dilatancy is a structural and not material effect. It appears to be no real increase in the volume of a concrete solid when the solid is placed under pressure.

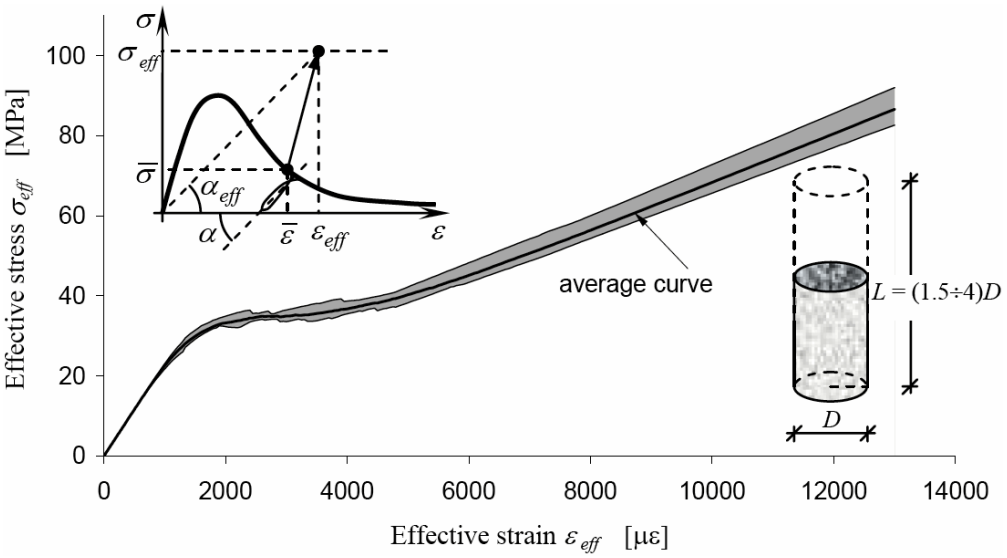

Figure 15: $\sigma_{eff} - \varepsilon_{eff}$ dispersion range for variable L/D ratio and average curve [Ferretti (2004a)]

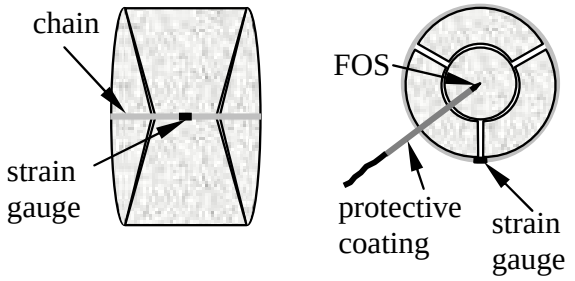

Figure 16: Positioning of strain gauge and FOS in the concrete specimen

It is worth noting that also in Brace Paulding and Scholz (1966) was assumed that part of the observed dilatancy, particularly of brittle rocks, might be due to splitting and open axial cracks, with cracks forming in the axial direction at a fraction of the maximum stress, leading to a volume increasing relative to elastic changes in a first stage, and, then, to dilatancy. Moreover, in Nemat-Nasser and Obata (1988), numerical results are provided, showing that crack growing leads to substantial dilatancy which quickly offsets the elastic volumetric contraction, leading to overall volumetric expansion as the axial compressive load is increased.

3 Displacements at constant load

As discussed in Section 1, the $\sigma - \varepsilon$ laws are usually derived from the $N - u$ laws by means of a scale factor. Thus, the inelastic and time-dependent behavior of u leads to an inelastic and time-dependent behavior of ε. In particular, the strain time-dependence at constant load, called the creep, is explained on the basis of the slips due to bond ruptures, with restorations at adjacent sites, in the hardened Portland cement paste [Bažant (2001)]. With these assumptions, the displacement time-dependence at constant load turns out to be caused by a constitutive property of concrete alone, the creep. On the other hand, since displacements consist in two quotes, one constitutive, and one related to crack openings, even at low stress levels (Section 2.2), the time-dependent behavior of u cannot be related solely to the creep. Crack openings surely play some role in the time-dependence of u.

Several models which combine the effects of nonlinear viscous strain evolution and crack nucleation and propagation have been developed in past years [Xiexing and Zhida (1994); Zhaoxia (1994); Zhou (1994); Bažant and Li (1997a; 1997b); Ozbolt and Reinhardt (2001); van Zijl Borst and Rots (2001); Barpi and Valente (2002); Mazzotti and Savoia (2003); Challamel Lanos and

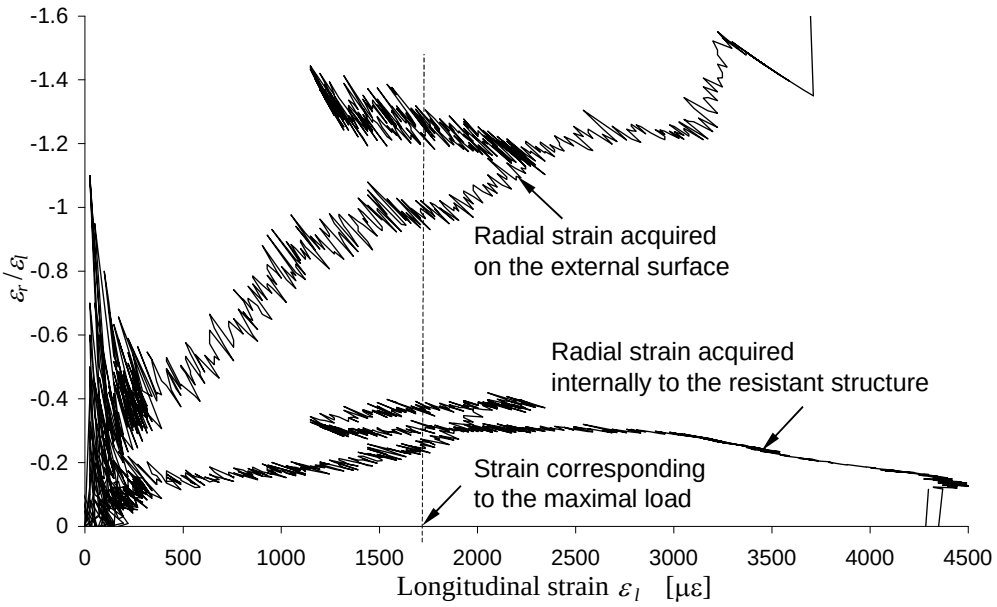

Figure 17: Ratios $\varepsilon_r/\varepsilon_l$: as conventionally defined and as presently proposed [Ferretti (2004b)]

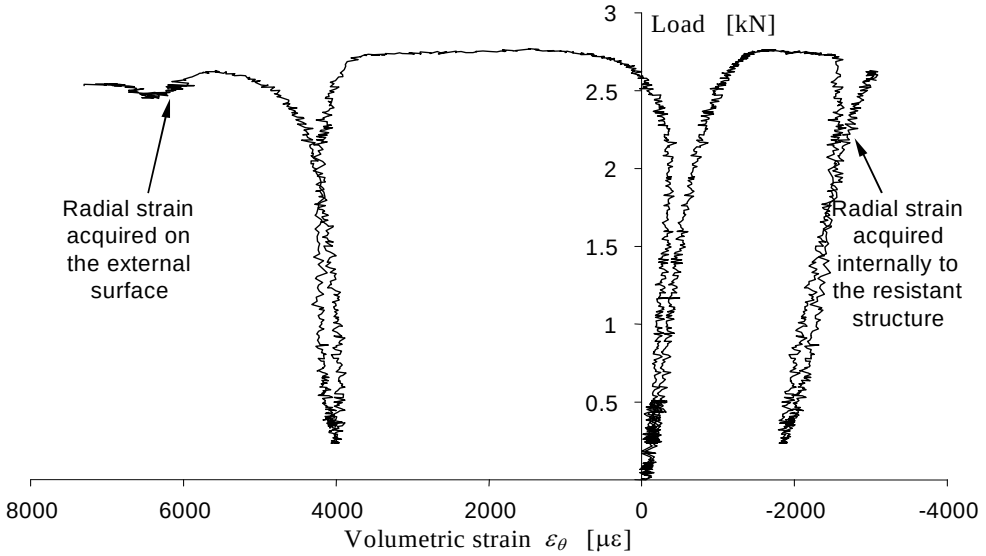

Figure 18: Traditional and identified volumetric curves for concrete specimens [Ferretti (2004b)]

Casandjian (2004); Ruiz Muttoni and Gambarova (2007)]. In the following Sections, results of an experimental program for defining the role played by cracking in the time-dependence of u are presented. The idea underlying the experimental program is that creep too may, partly, be a structural (and not the material) effect. That is, the time-dependence of u could be caused, mostly, not by material creep, but by crack propagation.

As it is well known, when the uniaxial compression test is interrupted, keeping the load constant under a certain value N_s (modality in load-control), the displacements do not cease to increase: a time-dependent behavior is observed, with the representative point P on the load-displacement diagram moving parallel to the displacement axis (Figure 19).

Two limit curves can be identified on the $N-u$ plane (Figure 20), the upper and the lower limit curves. These curves differ from each other for

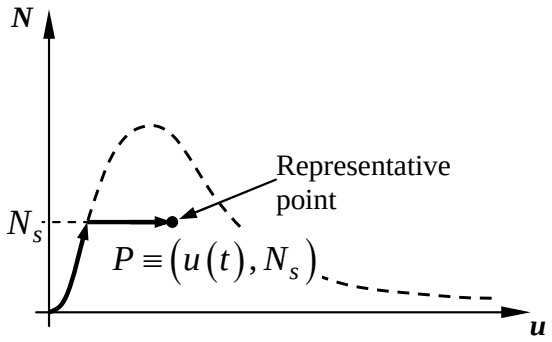

Figure 19: Time-dependent displacement development at the constant load N_s

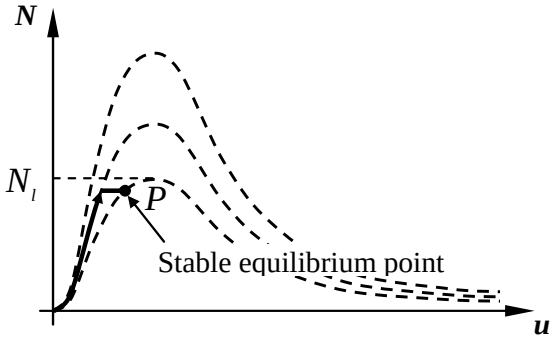

Figure 21: Trajectory of the representative point P for $N_s < N_l$

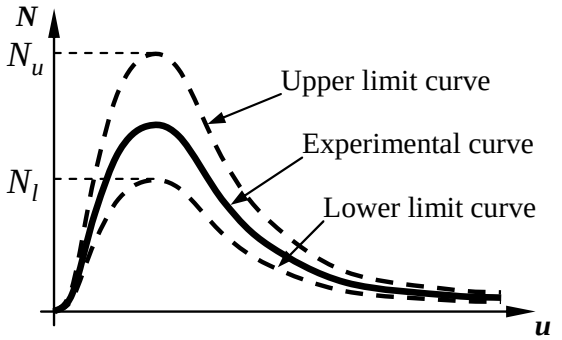

Figure 20: Limit curves in the load-displacement plane

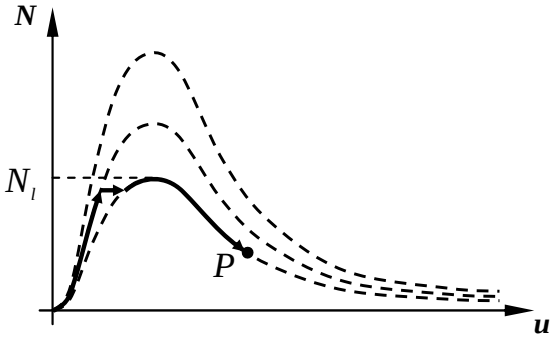

Figure 22: Trajectory of the representative point P for infinitely slow loading, after load stabilization under $N_s < N_l$

the rate of displacement increasing during loading: the lower limit curve is the locus of equilibrium points for infinitely slow loading, while the upper limit curve is the equilibrium curve obtained for high-sustained load. The portion of plane between the two limit curves defines the equilibrium domain in the $N-u$ space and the two limit curves are the boundary of this domain. Both the limit curves are softening for standard cylindrical specimens ($D = 15$ cm; $L = 30$ cm), with a maximum load equal to N_l for the lower and N_u for the upper (Figure 20).

Depending on the value of N_s, when the representative point P of Figure 19 moves at constant load, it can reach the lower or the upper limit curve.

If $N_s < N_l$, the representative point reaches the ascending branch of the lower limit curve (Figure 21), the displacement stops to increase at constant load, and a stable equilibrium condition is reached (displacement stabilized under the load $N_s < N_l$). Further displacement increase is possible only if the load is increased. In this case, the point P moves from the stable equilibrium point, following a curve which depends on the rate of displacement increasing once more: for infinitely slow loading, the point P moves along the lower limit curve (Figure 22), while, for high-sustained load, the point P moves along a bifurcation softening curve, inside the stability domain (Figure 23).

If $N_s \geq N_l$, the representative point reaches the softening branch of the upper limit curve in a point which is of unstable equilibrium (Figure 24): if the load-control modality is converted to displacement-control modality as soon as P reaches the upper limit curve and the load decreased, the point P moves along the softening branch of the upper limit curve (Figure 24), and if

it is not, the specimen is crushed (unstable equilibrium condition).

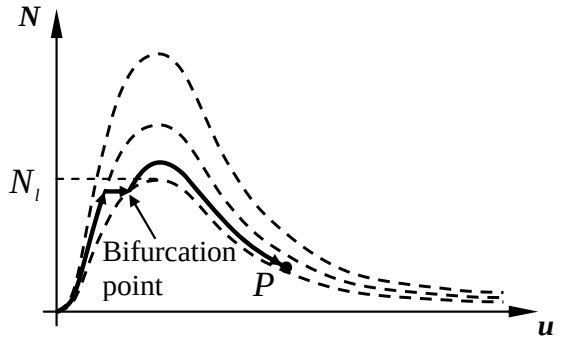

Figure 23: Trajectory of the representative point P for high-sustained loading, after load stabilization under $N_s < N_l$

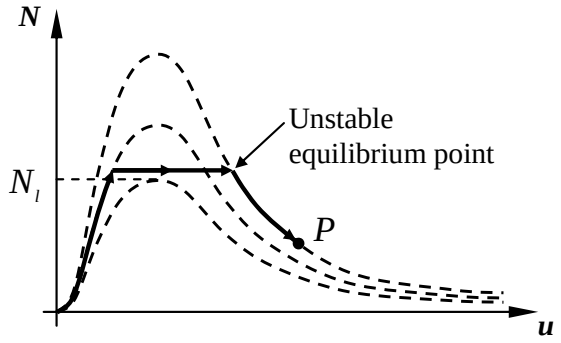

Figure 24: Trajectory of the representative point P for $N_s \geq N_l$

In conclusion, the time-dependent growth of displacements is stable in the ascending branch and unstable in the softening branch of an infinitely slow loading curve. This, together with the fact that, according to the findings of Nemat-Nasser and Horii (1982), as the peak axial load is approached, the crack growth becomes unstable, due to the small lateral tension at the crack tip following from the mixed-mode crack propagation (Figure 5b), may let us suppose that time-dependency of displacements at constant load is somehow connected to cracking. Figure 11 too supports this hypothesis: since the slope of the curve in Figure 11 gives the rate of cracking with the axial displacement, we can appreciate how the rate of cracking dramatically increases at the flex point in Figure 11, which occurs just at the peak axial load. The aim of the experimental program presented in the following Section is just to explore the relationship between time-dependence of displacements at constant load and cracking.

3.1 Experimental program

In order to investigate the role played by cracking in displacement time-dependence, a compression test in uniaxial loading has been performed, with evaluation of the time-dependence of both the displacements and the failure patterns, at two levels of constant load, N_{s1} and N_{s2}. Due to the low data dispersion of the effective law (Section 2.2), the compression test was performed on one specimen only. A cylindrical specimen with a diameter of 15 cm and a high of 30 cm was used. The first and second value of constant load, N_{s1} and N_{s2}, were fixed in order to reach the lower limit curve and the softening branch of the upper limit curve, respectively ($N_{s1} < N_l$, $N_{s2} \geq N_l$).

The compression test was performed in five stages (Figure 25):

1. The load was increased until the value N_{s1}, (modality in displacement-control).
2. The load was kept equal to N_{s1} until the lower limit curve was reached (modality in load-control).
3. An unloading-reloading cycle was performed for the load N_{s1}. Afterwards, the specimen was loaded until the value N_{s2} (modality in displacement-control).
4. The load was kept equal to N_{s2} until the softening branch of the upper limit curve was reached (modality in load-control).
5. The softening branch of the upper limit curve was followed until crushing (modality in displacement-control).

In order to evaluate the nature of time-dependent displacements, only acquisitions in the second and forth stages are significant. In these two stages, the acceptability threshold of the added

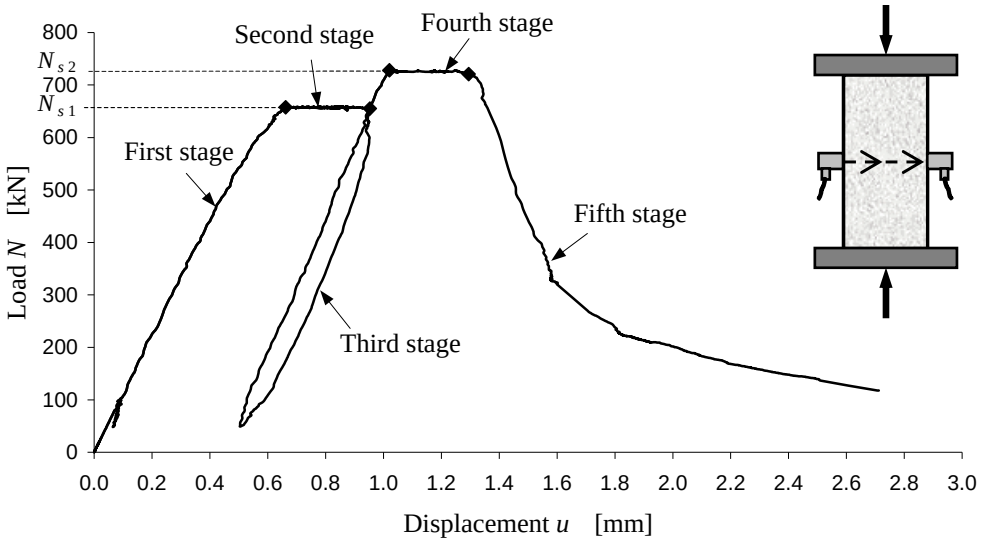

Figure 25: Stages of the load-carrying process for the tested cylinder

noise (Figure 11) has not yet been reached, and both d_1 and d_2 can be used for evaluating the percentage decrease of resistant area (Eqs.(5) and (6)).

The reloading branch of third stage intersects the branch of second stage in its end point (Figure 25). That is, when the load N_{s1} is recovered, the displacement of third stage equals the final displacement of second stage. This happens since the lower limit curve was actually reached at the end of the second stage, and no further time-dependent displacements developed during the unloading-reloading cycle. During the second stage, the time-dependent displacements were stabilized under the load N_{s1}, and a stable equilibrium condition was reached. Further time-dependent displacements are only possible if a load greater than N_{s1} is charged on the specimen. When the unloading-reloading cycle is performed without leaving the displacement to stabilize before unloading, the reloading branch does not pass through the unloading point. In this case, an additional displacement is measured when approaching the unloading load. If the unloading point is in the ascending branch of the load-displacement diagram, the unloading load can be recovered. If the unloading point is in the softening branch of the load-displacement diagram, the reloading branch intersects the load-displacement diagram for a load that is lower than the unloading load. In this case, the unloading load cannot be recovered and the representative point can move on the load-displacement diagram from the intersection point on. Such a situation is schematized by the dotted cycle in Figure 12.

Note also that the reloading branch of third stage does not exhibit a non-linear behavior approaching N_{s1} (Figure 25). On the contrary, the branch of first stage approaches N_{s1} in a non-linear manner (Figure 25). The difference between these two branches lies in the fact that, in the first stage, the load is increased without leaving the displacement to stabilize, while, in the third stage, a displacement stabilization has occurred under the unloading load. Thus, the development of time-dependent displacements is exhausted in the third stage, while not in the first stage. Consequently, in the first stage, the time-dependent displacements activated for a certain value of load superimpose to the elastic and time-dependent displacements due to load increasing. Comparing the non-linear behavior of first stage (with displacements superimposition) with the linear behavior of third stage (with no displacements superimposition), it can be concluded that the non-linearity of first stage is due to time-dependent effects. In the assumption that time-dependence is due to crack propagation, it finally follows that the non-linearity

of first stage arises for crack initiation. Thus, the non-linearity of first stage is not constitutive. This does not mean that the non-linear constitutive behavior of concrete does not exist. We can only state that the crack-induced non-linearity is predominant on the constitutive-induced non-linearity of first stage.

3.2 Identification of the effective law

In Figure 26, the curve of the effective law, which turned out to be monotonic non-decreasing, is compared with the curve of the average values. Also the correspondence between average and effective points is provided for the points delimiting the five load stages and two points in the softening branch of the average curve. For clarity of representation, the effective law is plotted without the unloading-reloading cycle of third stage.

Since the final strain is greater than the acceptability threshold of the added noise (Figure 11), the effective curve in Figure 26 has been derived by means of d_1, (Eq. (5)).

From Figure 26, it can be appreciated that the first stage of the effective law is quite linear. Thus, the identifying procedure confirms that the non-linearity of first stage is not constitutive, such as was concluded on the basis of the reloading branch of third stage (Section 3.1).

Since the load has been kept constant under the values N_{s1} and N_{s2} until the lower and upper limit curves have been reached, respectively, four discontinuities arise in the derivative of the average curve (Figure 26), due to the change of load-carrying modality. No discontinuity in the constitutive law is expected during the transition of load-carrying modality, of course, since it can be asserted that a properly consistent identification procedure from load-displacement to stress-strain should lead to a curve without discontinuity points for transitions of load-carrying modality. As can be seen in Figure 26, no discontinuity actually appears in the effective curve. This gives a further validation to the proposed identification procedure.

The absence of discontinuities in the transition points of the effective curve comes from the sensitivity of d_1 to the load-carrying modality (Figure 27). In other words, the modality transition is entirely charged by the law describing the decreasing of the resistant area. In Figure 27, the discontinuity in the d_1 law for the transition between the second and third and between the third and fourth stages is well evident. When the effective stress is evaluated in accordance with Eq. (7), the discontinuous behavior is discarded from the law $N = N(u)$ by means of the law $A_{res} = A_{res}(u)$.

From Figure 27, it can also be appreciated that, in the unloading branch of third stage, d_1 (A_{res}) is increasing (decreasing) at first, and then decreasing (increasing). The decreasing behavior of d_1 at the end of the unloading can be explained on the basis of a partial crack closure, leading to compressive stresses that are transmitted by the re-closed crack edges and, thus, to a partial A_{res} recovering. The crack edges re-open as soon as the load (average strain) is re-increased, and the A_{res} recovering is lost. In Figure 27, it is clearly evident how A_{res} equals the lower A_{res} of unloading as soon as the load-carrying process is inverted and the load (average strain) re-increased. After the crack edges re-opening, the value of A_{res} remains constant until the load N_{s1} is recovered (Figure 27). The constancy of A_{res} from the re-opening point up to the point in which N_{s1} is recovered means that no crack propagation characterizes this phase. On the other hand, this is also the phase in which time-dependent displacements have stabilized under the first value of load, N_{s1}. That is, no crack propagation is accompanied by no time-dependent displacements. Consequently, it seems that a strict relationship exists between crack propagation and time-dependent displacements.

3.3 Acquisitions at constant load

For the stages at constant load, the displacement versus time has been compared with the cracking versus time, where the displacement is the relative displacement between the platens of the testing machine, and the amount of cracking has been evaluated as the percentage decrease of A_{res}, by means of Eqs. (5) and (6). Since d_1 and d_2 are directly proportional to the dissipated energy and

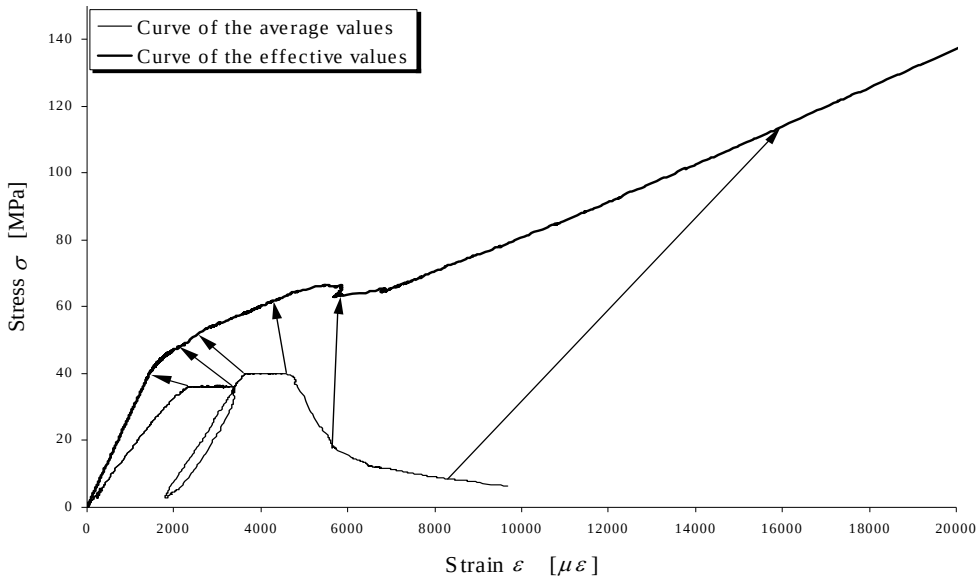

Figure 26: Comparison between the curves of the average and effective values

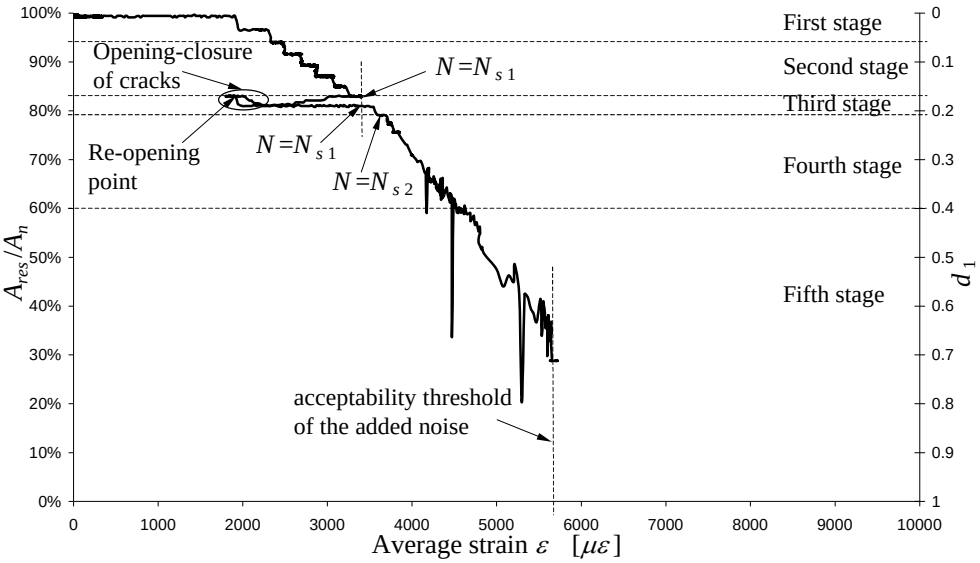

Figure 27: Evolution of the resistant area with the average strain

the microseismic velocity, respectively, W_d and V have been assumed as the representative parameters of cracking to compare with displacements at constant load.

As previously shown, in the second stage displacements have stabilized under the first value of load, N_{s1}. This means that the incremental displacement at infinity time for the load N_{s1} is equal to zero. Thus, the lower limit curve is reached at infinity time. Waiting for a displacement stabilization at infinity time is impossible, of course. Thus, it is necessary to fix a control range of time as the minimum time range during which a displacement must remain constant (within a certain tolerance) in order to consider it as stabilized. The control range of time depends on the single test. It can be estimated to be within an order of hours. A very long acquisition time is then needed in the second stage, if compared to the acquisition time needed in the other stages.

This may lead to saturation of the data acquisition board. Moreover, the rate of displacement increasing in the second stage is slower than in the other stages, the closer one gets to the lower limit curve. It follows that a lower acquisition rate is needed in the second stage, the closer one gets to the lower limit curve. In order to avoid saturation problems and optimize acquisition, the operator is requested to change the acquisition rate in the second stage, decreasing it the closer one gets to the lower limit curve. For deriving representative laws of data time-evolving, the acquired points have been equally spaced out on a modified axis of time. Such a type of modified axis of time is scaled from the axis of the acquisition step. All diagrams presented in this paragraph are plotted as acquired datum versus acquisition step.

The comparisons between displacement and dissipated energy and between displacement and microseismic velocity have been plotted in Figure 28 and Figure 29, respectively. In Figure 28, the number of acquisition steps is greater than in Figure 29, since the acquisition of the microseismic velocity was stopped as soon as the acceptability threshold of the added noise was reached (fifth stage). The scales of displacements, dissipated energy and microseismic velocity have been calibrated in order to compare the laws of displacements, dissipated energy and microseismic velocity directly on the plot. For clarity of representation, only data relative to the range $N_{s1} \leq N \leq N_{s2}$ have been plotted in the third stage.

The first stage in Figure 28 (Figure 29) is the stage in which displacements increase in accordance with the constitutive law. No crack initiation characterizes this stage, apart from the very end of the stage itself. The value of dissipated energy and microseismic velocity is, thus, almost constant, while displacements increase with the acquisition step. The final part of the first stage is affected by crack initiation and propagation. In the third stage, with $N_{s1} \leq N \leq N_{s2}$, displacements increase in accordance both with the constitutive law and the failure process. In this stage too, thus, we cannot expect to find a relationship between the increase (decrease) of dissipated energy (velocity) and the increase of displacement.

In the second stage, increases of displacement for load increasing do not occur. Thus, displacements only increase for crack propagation (structural effect) and creep (constitutive effect). In this stage, the two diagrams in Figure 28 and Figure 29 are close to each other. Also in the fourth stage, displacements only increase for crack propagation and creep. The two diagrams would superimpose in the fourth stage too, with adequate scale re-calibration. We cannot have a contemporary superimposition in the second and fourth stages, due to the displacement for load increasing that occurred in the third stage. This displacement afflicts the law of displacement versus acquisition step, while not the laws of dissipated energy and velocity versus acquisition step, modifying the scale factor between displacement and dissipated energy and between displacement and velocity. This means that it is possible to bring in direct relationship displacement and dissipated energy (velocity) both in the second and fourth stages. That is, when displacements increase with time at constant load, also the dissipated energy (velocity) increases (decreases) with time, and the two laws are directly related to each other. Thus, each increase of displacement is directly related to a proportional increase (decrease) of dissipated energy (velocity). No change in displacements occurs if no change in dissipated energy (velocity) occurs and any change of displacement is directly related to a change of dissipated energy (velocity).

Due to the direct relationship between W_d and d_1 (Eq. (5)) and between V and d_2 (Eq. (6)), it can finally be stated that it is possible to bring time-dependent displacements and resistant area in direct relationship to each other. In other words, if the creep is the time-dependence at constant load of the average strain (and, thus, of the axial displacement), as usual, it can be stated that it is possible to establish a direct relationship between creep and cracking. This is in total agreement with the experimental program of Meyers, Floyd and Slate (1969), where the relationship between crack length and average strain at constant load was found to be linear. In Meyers, Floyd and Slate (1969), the linear relationship between crack length and average strain at constant load was

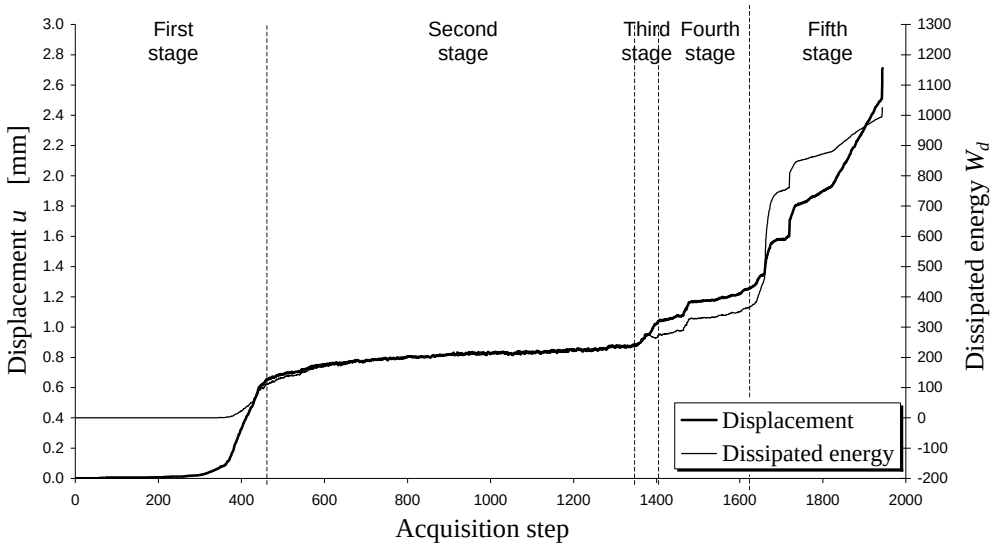

Figure 28: Comparison between displacement and dissipated energy versus the acquisition step

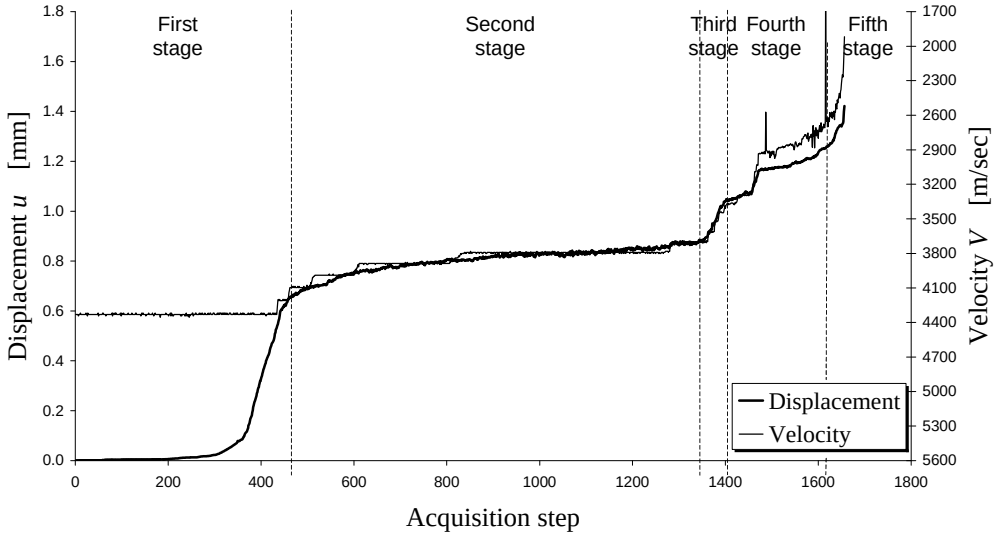

Figure 29: Comparison between displacement and velocity versus the acquisition step

explained as the increase in cracking caused by creep. Here, we propose to interpret the same experimental result as the increase in displacements at constant load caused by cracking, where the displacements increase at constant load not only for the creep, but also for the voids originated by the cracking itself. That is, creep is mostly an apparent and not constitutive effect, induced by cracking at constant load. The propagation of internal microcracks with increasing creep is also confirmed by the experimental program on the effective Poisson's ratio of Zhaoxia (1994).

Note that the stabilization of displacements in the second stage is accompanied by stabilization of resistant area. Actually, both displacements and dissipated energy (velocity) admit an horizontal asymptote when approaching the end of the second stage (Figure 28, Figure 29). Since displacement stabilization occurs for any point of the first stage, it seems that a stable crack propagation characterizes this stage ($N < N_l$). That is, for $N < N_l$ a crack propagation activates, leading to a new equilibrium configuration. This propagation seems to be the major element responsible for

the increasing of displacements with time, when $N < N_l$, since the law of dissipated energy (velocity) versus acquisition step can be superimposed on the law of displacement versus acquisition step. The superimposition persists in the fourth stage, after adequate shifting, confirming the strict bond existing between time-dependent displacements and crack propagation. Anyway, this second time crack propagation is not stable, and structural instability arises when the upper limit curve is reached. Instability arising is evident from Figure 28 and Figure 29, since a more than proportional displacement increasing is appreciated in the fifth stage.

It may now be argued that the microseismic velocity could be sensitive to the viscosity flow. In this case, a variation of velocity at constant load could be related to creep and not to crack propagation. That is, at constant loads Eq. (6) could not provide a measure of resistant area, but of creep. Nevertheless, since the law of velocity decreasing at constant load is the same as the law of the energy increasing at constant load, we can state that a resistant area is actually measured from the velocity decreasing at constant load.

The relationship between crack propagation and displacement increasing is difficult to define. Anyway, after adequate scale calibration, the curves in Figure 28 and Figure 29 superimpose in the stages at constant load, the second and fourth stages, with variations of displacement strictly related to variations of resistant area and contemporaneous stabilization of displacements and crack propagation. This is sufficient to state that the time-dependence is strictly related to crack propagation.

These results do not allow evaluation of the viscous nature of concrete. Neither is it possible to answer the question of whether creep really exists or not. Anyway, the superimposition allows one to state that, if creep exists in concrete, its contribution to the time-dependent behavior at constant load is not significant. Quantitatively, any displacement increase due to creep is much smaller than the displacement increase due to crack openings.

4 Conclusions

Studies by previous Author's on constitutive parameters identification seem to indicate that the final stage in compressed concrete specimens is mostly characterized by propagation of a macro-crack, rather than by crushing. This failure mechanism leads to reconsider the traditional identification of stress-strain and volumetric diagrams, attributing these diagrams to a structural and not to a constitutive behavior. Actually, the propagation of the macro-crack involves a discontinuity in the displacement field, with rigid displacements due to crack openings. For such a type of model it is no longer possible to consider the specimen as uniformly stressed and strained. Therefore, it is no longer possible to identify the constitutive properties from the experimental data through mere scale factors. All the average quantities loose their physical significance. In particular, the relative displacement between the platens is a quantity related to the specimen, which behaves as a structure. The relative displacement is composed by two quotes, one related to material and one related to crack openings. Thus, there is no physical sense in dividing this displacement by the distance between the platens, in order to derive a material property. The division gives a quantity that is not related to material only, that is, is not a strain. In this context, speaking of strain time-dependence at constant load (creep) may not be correct.

The experimental time-dependence of displacements is an evidence. Nevertheless, speaking of strain time-dependence is only possible if the identification process from displacements to strains is known. In other words, if the idea of uniform stress and strain is abandoned, creep must be put on new foundations. The existence of creep itself may be under question.

An experimental program has been performed, in order to get a better understanding of the phenomena involved in the time-dependent behavior of concrete. To this aim, attention has been focused on data acquisition for two values of constant loads. For these values of load, displacement and microseismic velocity have been ac-

quired until the limit curves have been reached. Also the dissipated energy has been computed. The dissipated energy and the microseismic velocity have been put in relationship with the decreasing of resistant area, due to crack propagation. This allowed comparison between displacement and crack propagation at constant load. The increasing of displacement at constant load has been found to be very close to the decreasing of resistant area at constant load. Time-dependence seems thus to be strictly related to crack propagation, rather than to creep. Also comparison between displacements and resistant area in the unloading-reloading cycles confirms the strict relationship between time-dependent displacements and crack propagation.

The existence of concrete creep is not confuted by these results, especially as far as the long-term mechanical response of reacting concrete is concerned [Suter and Benipal (2006)]. Anyway, these results are sufficient to conclude that creep plays a very limited role in the short- and medium-term mechanical response of non-reacting concrete. Displacement time-dependence in concrete specimens is mainly a structural effect due to crack propagation, which is stable for the ascending and unstable for the softening branches of the load-displacement diagram. Creep is a material property that has no significant effect on the macroscopic behavior.

Acknowledgement: This work was made possible by the Italian Ministry for Universities and Scientific and Technological Research (MURST). All the results here presented are part of the CIMEST Scientific Research on Identification of Materials and Structures – DISTART – Faculty of Engineering – University of Bologna – Alma Mater Studiorum.

References

Barpi, F.; Valente, S. (2002): Creep and Fracture in Concrete: a Fractional Order Rate Approach. *Engineering Fracture Mechanics*, vol. 70, pp. 611-623.

Bažant, Z.P. (2001): Creep of Concrete. In: K.H.J. Buschow, (Eds), *Encyclopedia of Materials: Science and Technology*, Elsevier, Amsterdam, vol. 2C, pp. 1797-800.

Bažant, Z.P.; Li, Y-N. (1997a): Cohesive Crack with Rate-Dependent Opening and Viscoelasticity: I. Mathematical Model and Scaling. *International Journal of Fracture*, vol. 86, pp. 247-265.

Bažant, Z.P.; Li, Y-N. (1997b): Cohesive Crack with Rate-Dependent Opening and Viscoelasticity: II. Numerical Algorithm, Behavior and Size Effect. *International Journal of Fracture*, vol. 86, pp. 267-288.

Bergan, P.G. (1983): Record of the Discussion on Numerical Modeling. *IUTAM W. Prager Symposium*, Northwestern University, Evanston, Ill.

Brace, W. F.; Paulding, B. W.; Scholz, C. (1966): Dilatancy in the Fracture of Crystalline Rocks. *J. Geophys. Res.*, vol. 71(16), pp. 3939-3953.

Candra, H.; Wright, W.J.; Albrecht, P. (2002): Experimentally determined key curves for fracture specimens. *International Journal of Fracture*, vol. 117, pp. 247-267.

Challamel, N.; Lanos, C.; Casandjian, C. (2004): Stability and Creep Damage of Quasi-Brittle Materials. *XXI International Congress of Theoretical and Applied Mechanics (ICTAM)*, Warsaw, Poland, August 15-21.

Daponte, P.; Olivito, R.S. (1989): Crack detection measurements in concrete. *ISMM International Conference Microcomputers Applications*, pp. 123-127.

Di Leo, A.; Di Tommaso, A.; Merlari, R. (1979): Danneggiamento per Microfessurazione di Malte di Cemento e Calcestruzzi Sottoposti a Carichi Ripetuti. *Technical Note 46* (in Italian), DISTART – University of Bologna, Italy.

Dresher, A.; Vardoulakis, I. (1982): Geometric softening in triaxial tests on granular material. Geotechnique, vol. 32, pp. 291-303.

Ferretti, E. (2001): *Modellazione del Comportamento del Cilindro Fasciato in Compressione*, Ph.D. Thesis (in Italian), University of Lecce, Italy.

Ferretti, E. (2003): Crack Propagation Model-

ing by Remeshing using the Cell Method (CM). *CMES: Computer Modeling in Engineering & Sciences*, vol. 4(1), pp. 51-72.

Ferretti, E. (2004a): Experimental Procedure for Verifying Strain-Softening in Concrete. *Int. J. Fracture* (Letters section), vol. 126(2), pp. L27-L34.

Ferretti, E. (2004b): On Poisson's Ratio and Volumetric Strain in Concrete. *Int. J. Fracture* (Letters section), vol. 126(3), pp. L49-L55.

Ferretti, E. (2005): A Local Strictly Nondecreasing Material Law for Modeling Softening and Size-Effect: a Discrete Approach. *CMES: Computer Modeling in Engineering & Sciences*, vol. 9(1), pp. 19-48.

Ferretti, E.; Di Leo, A. (2003): Modelling of Compressive Tests on FRP Wrapped Concrete Cylinders through a Novel Triaxial Concrete Constitutive Law. *SITA*, vol. 5, pp. 20-43.

Hallbauer, D.K.; Wagner, H.; Cook, N.G.W. (1973): Some observation concerning the microscopic and mechanical behaviour of quartizite specimens in stiff, triaxial compression tests. *International Journal of Rock Mechanics and Mining Sciences, Geomech. Abstr.*, vol. 10, pp. 713.

Hegemier, G. A.; Read, H. E. (1983): Some Comments on Strain-Softening. *DARPA-NSF Workshop*, Northwestern University, Evanston, Ill.

Horii, H.; Nemat-Nasser, S. (1985): Compression-induced microcrack in brittle solids: axial splitting and shear failure. *Journal of Geophysical Research*, vol. 90(B4), pp. 3105-3125.

Hudson, J. A.; Brown, E. T.; Fairhurst, C. (1971): Shape of the Complete Stress-Strain Curve for Rock. 13^{th} *Symposium on Rock Mechanics*, University of Illinois, Urbana, Ill.

Mazzotti, C.; Savoia, M. (2003): Nonlinear Creep Damage Model for Concrete under Uniaxial Compression. *Journal of Engineering Mechanics, ASCE*, vol. 129(9), pp. 1065-1075.

Meyers, B.L.; Slate, F.O.; Winter, G. (1969): Relationship Between Time-Dependent Deformation and Microcracking of Plain Concrete. *American Concrete Institute Journal & Proceedings*, vol. 69(1), pp. 60-68.

Nemat-Nasser, S.; Horii, H. (1982): Compression-induced nonplanar crack extension with application to splitting, exfoliation, and rochburst. *Journal of Geophysical Research*, vol. 87(B8), pp. 6805-6821.

Nemat-Nasser, S.; Obata, M. (1988): A microcrack model of dilatancy in brittle materials. *Journal of Applied Mechanics*, vol. 110, pp. 24-35.

Ozbolt, J.; Reinhardt, H.W. (2001): Three-Dimensional Finite Element Model for Creep-Cracking Interaction of Concrete. In: Ulm, Bažant & Wittmann (Eds.), *Proceedings of the sixth international conference CONCREEP-6@MIT*, Cambridge, England, Elsevier, Amsterdam, pp. 221-228.

Ruiz, M.F.; Muttoni, A.; Gambarova, P. (2007): Relationship Between Nonlinear Creep and Cracking of Concrete under Uniaxial Compression. *Journal of Advanced Concrete Technology*, vol. 5(3), pp. 383-393.

Sandler, I.; Wright, J. P. (1983): Summary of Strain-Softening. *DARPA-NSF Workshop*, Northwestern University, Evanston, Ill.

Soga, N.; Mizutani, H.; Spetzler, H.; Martin, R.J. III (1978): The effect of dilatancy on velocity anisotropy in Westerly granite. *Journal of Geophysical Research*, vol. 83, pp. 4451-4458.

Suter, M.; Benipal, G. (2006): Time-dependent behaviour of reacting concrete – I: Mechanism and theory. *Mech. Time-Depend. Mater*, vol. 10, pp. 51-62.

van Zijl, G.P.A.G.; Borst, R.; Rots, J.G. (2001): The Role of Crack Rate Dependence in the Long-Term Behaviour of Cementitious Materials. *International Journal of Solids and Structures*, vol. 38, pp. 5063-5079.

Wu, F. H.; Freud, L.B. (1984): Deformation trapping due to thermoplastic instability in one-dimensional wave propagation. *Journal of the Mechanics and Physis of Solids*, vol. 32(2), pp. 119-132.

Xiexing, M.; Zhida, C. (1994): A Creep Damage Equation for Rocks. *Acta Mechanica Solida*

Sinica, vol. 7(4), pp. 318-322.

Zhaoxia, L. (1994): Effective Creep Poisson's Ratio for Damaged Concrete. *International Journal of Fracture*, vol. 66(2), pp. 189-196.

Zhou, F.P. (1994): Numerical Modelling of Creep Crack Growth and Fracture in Concrete. In: *Localized Damage III Computer Aided Assessment and Control*, M.H. ALIABADI, Wessex Institute of Technology, Southampton, U.K, A. CAPPINTERI, Politecnico di Torino, Torino, Italy, S. KALISZKY, International Centre for Mechanical Sciences, Udine, Italy & D.J. CARTWRIGHT, Bucknell University, Lewisburg, USA, vol. 6.